Published in final edited form as:
Clin Cancer Res. 2013 January 1; 19(1): 158–169. doi:10.1158/1078-0432.CCR-12-2380.

Molecular Imaging Reveals a Role for AKT in Resistance to Cisplatin for Ovarian Endometrioid Adenocarcinoma

Hanxiao Wang[1,2,3], **Stefanie Galbán**[1,2,4], **Rong Wu**[5], **Brittany Bowman**[1,6], **Amanda Witte**[1,2], **Katrin Vetter**[1,2], **Craig J. Galbán**[1,4,7], **Brian D. Ross**[1,4,6,7], **Kathleen R. Cho**[4,5], and **Alnawaz Rehemtulla**[1,2,3,4]

[1]Center for Molecular Imaging, University of Michigan Medical School, Ann Arbor, MI

[2]Department of Radiation Oncology, University of Michigan Medical School, Ann Arbor, MI

[3]Cellular and Molecular Biology Program, University of Michigan Medical School, Ann Arbor, MI

[4]Comprehensive Cancer Center, University of Michigan Medical School, Ann Arbor, MI

[5]Department of Pathology, University of Michigan Medical School, Ann Arbor, MI

[6]Department of Biological Chemistry, University of Michigan Medical School, Ann Arbor, MI

[7]Department of Radiology, University of Michigan Medical School, Ann Arbor, MI

Abstract

Purpose—Ovarian cancer is the fifth leading cause of cancer deaths among American women. Platinum-based chemotherapy, such as cisplatin, represents the standard of care for ovarian cancer. However, toxicity and acquired resistance to cisplatin have proven challenging in the treatment of ovarian cancer patients.

Experimental Design—Using a genetically engineered mouse (GEM) model of ovarian endometrioid adenocarcinoma (OEA) in combination with molecular imaging technologies, we studied the activation of the AKT serine/threonine kinase in response to long-term cisplatin therapy.

Results—Treatment of cells in culture and tumor-bearing animals with cisplatin resulted in activation of AKT, a key mediator of cell survival. Based on these results we investigated the therapeutic utility of AKT inhibition in combination with cisplatin, which resulted in enhanced and prolonged induction of apoptosis and in significantly improved tumor control compared to either agent alone.

Conclusion—These results provide an impetus for clinical trials using combination therapy. To facilitate these trials, we also demonstrate the utility of diffusion-weighted MRI as an imaging biomarker for evaluation of therapeutic efficacy in OEA.

Keywords

bioluminescence imaging; diffusion-weighted MR imaging; ovarian carcinoma; AKT; cisplatin

Corresponding Author: Alnawaz Rehemtulla, PhD. Division of Molecular Imaging, Department of Radiation Oncology, University of Michigan Medical School. 109 Zina Pitcher Pl. Ann Arbor, MI. 48109. TEL: (734)-764-4209; FAX: (734)-763-5447; alnawaz@umich.edu.

Disclosure of Potential Conflict of Interest: B.D. Ross and A. Rehemtulla have ownership interest (including patents) from ImBio, LLC. B.D. Ross, A. Rehemtulla, have a financial interest in the underlying diffusion-weighted MR imaging technology. The other authors disclosed no potential conflicts of interest.

Introduction

Among American women, ovarian cancer remains the fifth leading cause of cancer related deaths with an estimated 22,280 new cases for the year 2012 (1). At diagnosis, nearly two thirds of women with ovarian cancer present with advanced stage disease, and their overall five-year survival is only 27% (2, 3). The vast majority of ovarian cancers are epithelial (carcinomas) and can be classified into four major subtypes, including serous, endometrioid, clear cell, and mucinous carcinomas (4). Recent efforts to better understand the genetic differences between these subtypes have shown that mutations predicted to dysregulate key signaling pathways characterize each subtype (5). For example, mutations of genes in the Wnt/β-catenin and PI3K/Pten signaling pathways co-occur in a substantial fraction of ovarian endometrioid adenocaraciomas (OEAs) (6). Although genetic differences in the subtypes of ovarian cancer have been recognized, surgical debulking followed by chemotherapy with taxanes and platinum-based drugs remains the first-line therapy for all subtypes (7). Unfortunately, even though most patients initially respond to treatment, tumors eventually relapse due to acquired drug resistance (8, 9). To overcome these hurdles, dose escalation studies have been explored but have been found intolerable due to toxicity and serious side-effects (10). Therefore, a better understanding of the mechanisms leading to drug resistance is urgently needed for the development of novel treatment paradigms to improve length and quality of life for ovarian cancer patients.

The cisplatin-resistant phenotype of cancer cells may be due to a number of mechanisms, including alterations that affect the intracellular uptake of cisplatin or altered sigaling pathways that ultimately impact the execution of the apoptotic program (10). The PI3K/AKT signaling pathway is important for cell survival, and plays a critical role in a number of other tumor-associated cellular processes, including cell growth, and cell cycle progression (11). Moreover, a recent study in cultured cells suggested that chemoresistance is mediated by AKT activation through DNA dependent protein kinase (DNA-PK) (12). However, limited work has been done to study the molecular basis of chemoresistance in a clinically relevant mouse model of ovarian cancer. We have previously described a genetically engineered mouse (GEM) model for OEA, which recapitulates the human disease more closely than traditionally utilized tumor xenograft models. In this model, simultaneous activation of canonical Wnt/β-catenin and PI3K/AKT signaling invariably leads to ovarian tumor development and is achieved by conditionally inactivating the *Apc* and *Pten* tumor suppressor genes in the ovarian surface epithelium of $Apc^{loxP/loxP};Pten^{loxP/loxP}$ mice (6). Tumors arise as early as three weeks post expression of Cre recombinase, and the utility of this model for testing novel therapies or treatment paradigms has been recently demonstrated (13).

Molecular imaging provides a unique opportunity to evaluate drug target interactions, induction of cell death, and tumor regression in a non-invasive and dynamic manner (14, 15). Using a bioluminescence reporter for AKT activity (16) and caspase-3 proteolysis (17), we provide evidence in the mouse model that the activation of the PI3K/AKT cell survival signaling pathway in response to cisplatin treatment contributes to resistance to cisplatin-induced apoptosis. Simultaneously, we here describe a new modification of our genetically engineered mouse model for OEA, wherein tumor specific caspase-3-dependent apoptosis can be imaged over time in response to therapeutic intervention. We provide validation studies for the use of diffusion-weighted MRI (DW-MRI) as an imaging surrogate for treatment efficacy and identified cisplatin in combination with perifosine as a therapeutic paradigm for future clinical trials.

Materials and Methods

Cell culture

Murine OEA-derived tumor cell lines were established by mechanically dispersing ovarian tumor tissues with sterile scalpels followed by digestion at 37°C with 0.05% Trypsin-EDTA for 20 minutes. Cells were cultured for five passages in DMEM containing 10% FBS/1% Penicillin/Streptomycin (P/S)/1% Insulin-Transferrin-Selenium (Invitrogen) in an incubator with 3% O_2/5% CO_2 (Model NAPCO 8000WJ, Thermal Scientific, Asheville, NC). During the first five passages of primary culture, all non-adherent cells were discarded, and only adherent cells were passaged. Adherent mesenchymal cells were removed by differential trypsinzation to further enrich the epithelial cell population. The Apc-/Pten- OEA-derived tumor cell line W2532T, denoted hereafter as W25, was maintained in DMEM medium (Gibco, Gaithersburg, MD) supplemented with 10% fetal bovine serum (Gibco). W25 cells display epithelial (cobblestone) morphology by light microscopy, and express epithelial markers cytokeratin 8 and 19 by immunofluorescence(13). Cre-mediated bi-allelic recombination of Apc and Pten in W25 cells was confirmed by PCR. To generate stable cell lines with bioluminescence reporters, W25 cells were transfected with plasmids (pEF apoptosis orAKT reporter) (16, 17) by using FuGENE 6 transfection reagent (Roche Diagnostics, Indianapolis, IN) following the manufacturer's instructions. Single clones stably expressing the reporters were maintained in DMEM medium with 10% FBS and 300μg/mL G418 (Invitrogen, CA).

Mouse Strains

Apc$^{loxP/loxP}$*;Pten*$^{loxP/loxP}$ mice have been previously described in detail (6). The transgenic bioluminescence-apoptosis reporter (*Apoptosis reporter*$^{tg/+}$) mouse was generated by the transgenic core of the University of Michigan. In brief, the Elongation Factor-1(EF1) promoter, which is widely and constitutively expressed, drives the transcription of the tdTomato coding sequence (a derivative of red fluorescent protein). The presence of a transcription stop site and poly-adenylation target site (pA) at the end of the tdTomato coding sequence results in termination of transcription such that only the tdTomato protein is expressed. In the presence of Cre recombinase, recombination of the loxP sequences results in deletion of the tdTomato coding sequence as well as the adjoining pA sequences. Cre recombination of the transgene results in transcription of the molecular imaging reporter as well as an internal ribosome entry site (IRES) and the renilla luciferase (rluc) coding sequence. A single mRNA from the transgene will express the reporter protein (apoptosis reporter) as well as the rluc protein.

Apc$^{loxP/loxP}$*;Pten*$^{loxP/loxP}$*;Apoptosis reporter*$^{tg/+}$ mice were generated by crossbreeding *Apc*$^{loxP/loxP}$*;Pten*$^{loxP/loxP}$ mice with *Apoptosis reporter*$^{tg/+}$ mice. All the animal experiments were done in accordance with protocols approved by University Committee on Use and Care of Animals of the University of Michigan (UCUCA protocol numbers 08669 and 09921).

Genotyping

Animals were genotyped using tail DNA. Genotyping primers used in this study are listed here: *Pten*$^{loxP/loxP}$ allele: forward primer 5′-CTCCTCTACTCCATTCTTCCC-3′ and reverse primer 5′-ACTCCCACCAATGAACAAAC-3′ (18); *Apc*$^{loxP/loxP}$ allele: forward primer 5′-GTTCTGTATCATGGAAAGATAGGTGGT-3′ and Reverse primer 5′-CACTCAAAACGCTTTTGAGGGTTGATTC-3′ (19); *Apoptosis reporter*$^{tg/+}$ allele: forward primer 5′-GAAGTATAGCAACAGAAGACGCCAAAAACATA-3′ and reverse primer 5′-CTAGAAATAGATCTCCCTCCTCCATCGACTTC-3′.

Western blot analysis

Cells were washed with phosphate-buffered saline (PBS) and lysed with NP-40 lysis buffer (1% NP40, 150 mM NaCl, and 25 mM Tris, pH 8.0) supplemented with protease inhibitors (Complete Protease Inhibitor Cocktail, Roche) and phosphatase inhibitors (PhosSTOP, Roche). Tumor tissues were collected at indicated time points, snap-frozen in liquid nitrogen, and stored at −80°C. Tissues were then homogenized in NP-40 lysis buffer supplemented with protease inhibitors and phosphotase inhibitors. Concentration of protein was determined using Lowry assays (Bio-Rad, Hercules, CA). Equal amount of protein was loaded in each lane and resolved by 4–12% gradient Bis-Tris gel (Invitrogen, CA). Proteins were transferred to 0.2 μm nitrocellulose membrane (Invitrogen, CA). Membranes were incubated overnight at 4°C with primary antibodies after blocking, followed by incubation with appropriate HRP-conjugated secondary antibody at room temperature for one hour. ECL-Plus was used to detect the activity of peroxidase according to the manufacturer's protocol (Amersham Pharmacia, Uppsala, Sweden). Antibodies raised against PARP, pAKT (Serine473 and Thr308), total AKT, pH2A.X(Ser139) and total H2A.X were purchased from Cell Signaling Technology (Beverly, MA).

Immunohistochemistry

After drug treatment, all mice were euthanized and tumor tissues were collected, fixed in 10% (v/v) buffered formalin, and embedded in paraffin. Immunohistochemical (IHC) staining for Ki67 was completed by the Tissue Core of the University of Michigan Comprehensive Cancer Center using standard techniques. Images from two representative 600X fields in the most cellular areas of tumors were acquired by Olympus BX-51 upright light microscope and an Olympus DP-70 high resolution digital camera (Olympus Corporation of the Americas, Center Valley, PA). Ki67 positive cells and negative cells were counted by ImageJ software (Wayne Rasband, National Institutes of Health, MD).

Bioluminescence imaging of cell culture

Cells were seeded at 5,000 cells/well in a 96-well dish. 24 hours post seeding, cells were incubated with indicated drugs for 20 hours prior to adding luciferin at a final concentration of 100 μg/ml. Luminescence was recorded by a luminometer (EnVision Xcite Multilabel Reader, PerkinElmer, Waltham, MA).

PI exclusion assay

Cell viability was determined by propidium iodide (PI) exclusion assay. PI was purchased from Invitrogen (Eugene, OR). Cells were seeded at 1×10^5 cells/ml. 24 hours post seeding, cells were incubated with indicated drugs for 48 hours prior to trypsinization and subsequently collection by centrifugation (400*g* for 3 minutes). PI staining solution was added at a final concentration of 0.1ug/ml. Percentage of PI positive cells was determined and recorded by BD FACSCanto™ Flow cytometry (BD Biosciences, San Jose, CA).

Allograft Implantation

6-week-old athymic female mice (CD-1 nu/nu, Charles River Laboratory, Wilmington, MA) were inoculated subcutaneously (s.c.) with 1×10^7 W25 cells expressing the bioluminescence reporters (apoptosis or Akt) into the flank on each side. Injections were a total volume of 200 μl cell suspension in 50% DMEM mixed with 50% BD Matrigel Matrix (Becton, Dickinson and Company, NJ). Caliper measurements were performed weekly to determine tumor volumes using the formula $V= (length/2)x(width^2)$ until s.q. tumors reached an approximate volume of 200 mm^3 at which time each animal was randomized into one of four treatment groups.

Intra-bursal injection

Replication-incompetent recombinant adenovirus expressing Cre recombinase (AdCre) under the control of the CMV promoter (20) was obtained from the University of Michigan's Vector Core. 5×10^7 plaque-forming units (p.f.u.) of AdCre were injected in a total volume of 5 μl containing 0.1% Evans blue (Sigma-Aldrich Inc., St. Louis, MO) into the right ovarian bursal cavity of 8- to 10-week-old female $Apc^{loxP/loxP};Pten^{loxP/loxP};$ *Apoptosis reporter* $^{tg/+}$ mice. Intrabursal injection was performed as previously described (21, 22). Each mouse's left ovarian bursa was untreated, thereby serving as control.

Drug administration

Control and perifosine-treated animals received vehicle or 10 mg/kg perifosine by intraperitoneal injection (i.p.), respectively, five times a week for two weeks with two days off in between treatment weeks. Animals in the cisplatin group received 2.5 mg/kg or 5 mg/kg cisplatin by i.p. injection twice a week for two weeks. For combination groups, mice were treated with 2.5 mg/kg or 5 mg/kg cisplatin twice a week with co-administration of 10 mg/kg perifosine.

In vivo Bioluminescence imaging

In vivo bioluminescence imaging was carried out by injecting tumor-bearing nude and genetically engineered mice intraperitoneally with 150 or 300 mg/kg of 40 mg/mL D-luciferin (Biosynth, Naperville, IL)/PBS solution, respectively, using an IVIS imaging system (Xenogen, Alameda, CA). Post injection mice were anesthetized with a 1–2% isoflurane/air mixture and serial images were acquired over 20–30 minutes to capture the peak photon emission for each animal. Regions of interest were drawn around the area of interest in each mouse and peak luminescence values of each series were used for analysis.

MR-Imaging

MR imaging on OEA mice was carried out on a 7T Agilent, Inc. (Palo Alto, CA) *Direct Drive* system with a quadrature mouse body volume coil (m2m Imaging Corp., Cleveland, OH). During all MRI procedures, animals were anesthetized with a 1–2% isoflurane/air mixture while maintaining body temperature using a heated air system (Air-Therm Heater, World Precision Instruments, Sarasota, FL). Anatomical MR images were acquired by a fast spin echo sequence with the following parameters: repetition time/echo time (TR/TE) =4000/15 ms, field of view (FOV)=40×30, matrix size=128×128, slice thickness=0.5 mm, echo train=8, echo spacing=15ms, and number of slices: 25~30. OEA mice were screened for tumor burden once per week from the fourth week post intra-bursal surgery. Mice were randomized into vehicle, cisplatin, perifosine or cisplatin plus perifosine group when their orthotopic tumor sizes reached approximately 50 mm^3. Mice were imaged by MRI twice weekly to followtumor sizes during treatment.

DW-MR images were obtained from a diffusion-weighted spin-echo sequence, with the following parameters: TR/TE = 2000/32 ms, FOV = 30×30, matrix size = 128×64, slice thickness = 1.0 mm, 10 slices, 2 averages, b-values (diffusion weighting) of 128 and 795 s/mm^2. Respiratory gating was performed using a monitoring system (Small Animal Instruments, Inc., Stony Brook, NY) to eliminate motion artifacts from breathing. DW-MRI scans were performed before treatment and seven days post treatment initiation.

Image Reconstruction and Analysis

Volumes of interest (VOIs) were manually contoured around the enhancing rim of the tumors on the anatomical images for measurements of tumor volume. To determine the whole-tumor means of ADC (apparent diffusion coefficient), VOIs were manually

contoured around the enhancing rim of the tumors on diffusion-weighted image slices at b=128 s/mm^2. ADC maps were calculated from the two diffusion weightings (b-values) using the following equation:

$$ADC=\ln\left(\frac{S_1}{S_2}\right)/(b_2-b_1)$$

where S_1 and S_2 are the signal intensities at b-values b_1 and b_2, respectively. Voxels that exhibited insufficient signal, defined as <10*noise, in the low b-value image (b = 128 s/mm^2) were excluded from the analysis. Subsequently, mean ADC values were calculated over the entire tumor volume. All image reconstruction and digital image analysis was accomplished using programs developed in Matlab (The Mathworks, Natick, MA, USA).

Results

Resistance to apoptosis in response to cisplatin is reversed by AKT inhibition

To study the mechanistic basis of cisplatin chemoresistance, we established a primary ovarian tumor cell line (W25) derived from our previously described murine OEA model (13). To enable imaging of caspase-3 activation, a surrogate for apoptosis, we generated a stable cell line (W25-Apop) expressing a previously described bioluminescent apoptosis reporter (17) as illustrated in Figure 1A.

The induction of apoptosis was evaluated using cultured cells in response to cisplatin alone (20 μM) or in combination with perifosine (30 μM), a small molecule inhibitor of AKT activity (23). As depicted in Figure 1B, combination therapy resulted in significantly elevated caspase-3 activation when compared to single agent as measured by an increase in bioluminescence signal. This finding was consistent with conventional western blot analysis for caspase-3 activity as measured by cleavage of PARP, which was only observed in response to combination therapy (Figure 1C). Additionally, we evaluated overall cell viability using PI exclusion assays (Figure 1D), wherein the combination therapy showed higher percentage of PI positivity compared to either agent alone.

To extend these studies *in vivo*, initial studies focused on following the treatment effects of subcutaneous W25-Apop tumors growing in athymic nude mice. Animals treated with vehicle, perifosine (10 mg/kg, 5 times a week), cisplatin (5 mg/kg, 2 times a week), or combination treatment of cisplatin (5 mg/kg, 2 times a week) and perifosine (10 mg/kg, 5 times a week) were studied using the bioluminescence molecular reporters. The greatest induction of apoptosis as measured by bioluminescence was observed in the cohort of animals treated with the combination of cisplatin and perifosine (Figure 2A and 2B). Treatment of tumor-bearing animals with perifosine resulted in enhanced bioluminescence signals (5 fold) on each day of treatment during the first week over the control group. Perifosine as a single agent failed to induce apoptosis during the second week (days 8–12). The combination of cisplatin and perifosine induced apoptosis to a similar extent as perifosine alone in the first week of treatment (5–6 fold) but a significant increase in apoptosis (10 fold) was observed in the second week of treatment (Figure 2A). A significant degree of toxicity as measured by loss of weight was observed in mice treated with cisplatin at 5mg/kg, twice a week. To further evaluate the efficacy of cisplatin and perifosine, we used a lower dose of cisplatin (2.5mg/kg, twice a week). At these doses we observed a similar enhancement of bioluminescence in the combination group, compared to cisplatin alone after the first day of treatment (Figure 2C). Furthermore, by the end of two weeks of treatment both cisplatin and perifosine as single agents showed significantly increased tumor volumes over baseline measurements while the combination treatment prevented tumor growth during the treatment period (Figure 2D). Cisplatin alone had some anti-tumor effect,

as tumors were smaller in cisplatin-treated mice than in mice treated with vehicle alone over the 2 week treatment period.

A role for AKT in resistance to cisplatin treatment

To investigate the regulation of AKT activity in live cells and animals, we used our previously described bioluminescence AKT reporter (BAR, Figure 3A). The reporter is designed such that increased bioluminescence activity is observed upon inhibition of the AKT-kinase (16). Using BAR-expressing W25 cells (W25-BAR) we evaluated AKTactivity in response to cisplatin and/or perifosine. As expected, perifosine treatment resulted in a significant increase of bioluminescence activity due to AKT inhibition. Unexpectedly, the combination of cisplatin and perifosine showed a six fold increase of bioluminescence, suggesting that cisplatin treatment elevated AKT kinase activity and that perifosine treatment resulted in a greater decrease in AKT activity (Figure 3B). This was confirmed by phospho-AKT western blot analysis which showed that both Ser473 and Thr308 phosphorylation was elevated upon cisplatin treatment in W25-BAR cells whereas perifosine treatment reversed AKT phosphorylation (Figure 3C). To investigate if this phenomenon was reproducible in tumors, AKT activity in response to therapies was evaluated in W25-BAR allografts. W25-BAR tumor-bearing animals were randomized into four groups consisting of control (vehicle), cisplatin (2.5 mg/kg, 2 times a week), perifosine (10 mg/kg, 5 times a week) or combination therapy when tumors reached 200mm^3 in volume. As shown in Figure 3D, treatment of s.q. tumor bearing mice with perifosine expectedly resulted in increased bioluminescence during treatment. In accordance with cell culture results, animals treated with the combination of cisplatin and perifosine showed a prolonged and enhanced increase in bioluminescence signal in the second week of treatment, indicative of enhanced AKT inhibition (and therefore activity). We hypothesized that repetitive cisplatin exposure during the first week of treatment elevated phospho-AKT levels in tumor allografts thereby allowed for increased bioluminescence signal to be detected due to simultaneous AKT inhibition. To test this hypothesis, tumor samples were collected following the first week (cycle) of therapy. Western blot analysis confirmed that cisplatin treatment resulted in an increase in AKT activation as measured by phospho-AKT. Combination treatment showed decreased levels of phospho-AKT compared to cisplatin alone indicating that perifosine treatment reversed the activation of AKT (Figure 3E).

AKT phosphorylation is regulated by various factors, including DNA damage caused by radiation and chemotherapies (12, 24). In order to evaluate the DNA damage response pathway following cisplatin treatment, phosphorylation of histone H2A.X levels were evaluated. As shown in Figure 3F, phospho-H2A.X was induced in cisplatin and combination treatment groups, indicating that cisplatin treatment resulted in DNA damage inducingAKT activation.

Imaging of apoptosis in a GEM model

The tumor microenvironment - including adjacent normal tissue, stromal cells, vasculature, lymph and immune cells - impacts the response of tumor cells to therapeutic intervention (25, 26). For the purpose of imaging apoptosis non-invasively in an ovarian cancer animal model, we generated a new reporter mouse by pronuclear microinjection of a transgene containing the apoptosis reporter into fertilized eggs obtained from FVB/N females. The schematic diagram shown in Figure 4A depicts the transgene apoptosis reporter construct. *Apoptosis reporter*$^{tg/+}$ transgenic animals were crossed with *Apc*$^{loxP/loxP}$; *Pten*$^{loxP/loxP}$ mice to generate *Apc*$^{loxP/loxP}$; *Pten*$^{loxP/loxP}$; *Apoptosis reporter*$^{tg/+}$ mice for use in subsequent experiments.

In this new OEA model with the built-in apoptosis imaging reporter, Cre-expression resulted in the deletion of both copies of *Apc* and *Pten* and expression of the apoptosis reporter in transformed ovarian surface epithelial cells. Mice injected with AdCre are referred hereafter as $Apc^{-/-}; Pten^{-/-}; Apopreporter^{+}$, indicating successful Cre-mediated recombination. Representative images of bioluminescence activity in $Apc^{-/-}; Pten^{-/-}; Apopreporter^{+}$ mice with ovarian tumors before and following one day of treatment are shown in Figure 4B. Bioluminescence signals were only detected in the right abdomen, indicative of tissue-specific activation of the apoptosis reporter upon AdCre injection into the right ovary. Consistent with our previous data obtained in cell culture and allografts, bioluminescence activity increased following combination therapy indicating activation of caspase-3 had occurred. Tumor progression in $Apc^{-/-}; Pten^{-/-}; Apopreporter^{+}$ animals was followed over time using MRI beginning at four weeks post AdCre injection. Once tumor volumes reached approximately $50mm^3$, animals were randomized into four treatment groups: vehicle, perifosine, cisplatin and combination therapy. Following treatment initiation, bioluminescence imaging was performed 6 hours post treatment on days 1, 5, 8 and 12. Apoptosis reporter activation was normalized to tumor volume changes by performing MRI at the same time points in which bioluminescence imaging was performed. As demonstrated in Figure 4C, the combination treatment of perifosine and cisplatin resulted in the highest and most sustained induction of bioluminescence when compared to vehicle treated or single agent treated animals, indicating maximum apoptotic cell kill was achieved. Similar to the data obtained from the allograft study, we observed an increase in the level of apoptosis in perifosine treated animals 6 hours post treatment initiation. As mentioned above, the initial surge in cell death upon phospho-AKT inhibition might be due to the cells' addiction to activated PI3K/AKT pathway. In fact, inhibition of the PI3K/AKT pathway in cancer cells has been shown to induce apoptosis (23). Although no caspase-3 activation upon single agent cisplatin treatment was observed using bioluminescence imaging, tumor growth was inhibited as assessed by MRI (Figure 4E) indicative of caspase-3 independent cytotoxicity due to the high dose of cisplatin which was also observed in our allograft study (Figure 2A). Quantitative analysis of the MRI data show tumor volumes were significantly reduced in the combinatorial treatment over all other treatment groups (Figure 4E), thus confirming our previous results using the OEA tumor allografts. Target inhibition by drug was confirmed by western blotting against phospho-AKT(Ser473) and total AKT of tumor tissues obtained from animals treated with perifosine. As depicted in Figure 4F, perifosine treatment resulted in a decrease in phospho-AKT levels at 3 hours post-treatment initiation.

DW-MRI can be used to measure changes in cellular density within tumor tissue and has been established as a clinically relevant surrogate imaging biomarker for treatment response assessment in cancer patients (27, 28). We performed DW-MRI on tumor-bearing mice in order to evaluate the effects the treatment as well as the ability of DW-MRI to detect and differentiate the effectiveness of each treatment. As shown in Figure 5A and Figure 5B, we observed a decrease in ADC values in vehicle and perifosine-treated animals after two weeks of treatment suggesting that perifosine alone is not efficacious in inducing cell death. The observed decrease in ADC values in vehicle and perifosine groups suggested that cells were undergoing active proliferation resulting in increased tumor cellularity over this time period. This finding was further supported by immunohistochemical analysis of tumors obtained from these animals one week after treatment initiation. Ki67 staining, indicative of cell proliferation, increased in vehicle and perifosine-treated animals as shown in Figure 5C and Figure 5D. However, cisplatin and combination treated animals showed increased ADC values (Figure 5A and Figure 5B) and decreased Ki67 staining (Figure 5D), which suggested that increased cell death was the likely cause of the resultant tumor regression as demonstrated in Figure 4E.

In summary, these studies revealed that combination treatment of cisplatin and perifosine was more efficacious than either drug alone in inducing apoptosis, and thereby tumor regression, by utilizing our new reporter mouse model of OEA in conjunction with non-invasive imaging modalities.

Discussion

Ovarian cancer patients treated with the chemotherapeutic agent, cisplatin, usually show an initial response yet ultimately succumb to their disease due to the development of resistance (10). Regulation of cellular drug uptake, increased DNA damage repair, and inhibition of apoptosis have been proposed to cause cisplatin resistance (29). The development of strategies for chemosensitization and prevention of therapeutic resistance remains a major goal with important clinical implications. Although a large body of work has been conducted towards this aim, the model systems typically employ cultured cells and/or immunocompromised mice bearing subcutaneous xenografts. In addition, analyses of molecular events in these model systems involves resection of tumor cells for *ex vivo* assays and thus provide only a non-quantitative snapshot of a dynamically changing and highly interactive cascade of signaling events following therapeutic intervention. The present study utilizes recent advances in genetically engineered mouse ovarian cancer models as well as the development of molecular imaging biomarkers which enable quantitative, non-invasive and temporal imaging of dynamic molecular events in living animals. Combining our tumor model systems with anatomical and molecular imaging approaches provided an opportunity to gain novel insights into the roles of PI3K/AKT signaling and the apoptotic machinery in the development of therapeutic resistance to cisplatin.

Our initial study utilized a mouse OEA cell line derived from an ovarian tumor which was engineered to express the apoptosis reporter. This line was subcutaneously implanted allowing for detection of caspase-3 activation in perifosine treated animals using bioluminescence imaging. While the imaging signal increased during the first week, a significant decline was observed during the second week of treatment. We reasoned that the cells' dependency on the PI3K/AKT pathway leads to an initial induction of apoptosis upon inhibition of AKT activity by perifosine, which may later be compensated by activation of alternate survival signaling pathways. In support, we and others have previously reported that AKT inhibition results in activation of compensatory signaling through MEK/ERK or other signaling pathways (13, 30). This finding may provide additional rationale for the simultaneous targeting of PI3K/AKT and MEK/ERK signaling pathways, but remains to be investigated for the treatment of OEA. Intriguingly, the caspase-3 reporter allowed us to determine that cell death and tumor regression induced by cisplatin in cell culture and in allografted or transgenic animals, respectively appeared to be largely caspase-3 independent. This is not surprising since cisplatin has been shown to exert its effects by inducing DNA damage, cell cycle arrest and ultimately necrotic cell death (31, 32) which serves to further validate the use of these molecular imaging reporters in the context of pre-clinical drug optimization studies.

Initial response to platinum-based therapies in the treatment of patients afflicted with ovarian cancer is usually high, yet most patients relapse due to acquired resistance. Recent studies by Stronach *et al.* comparing cisplatin-resistant and cisplatin-sensitive cell lines revealed a significant increase in phosphorylated AKTupon cisplatin treatment. AKT inhibition sensitized resistant cells to cisplatin, whereas inhibition of AKT in cisplatin sensitive lines had little effect on caspase-3/7 induction (12).With the ability to image and thus quantify AKT and caspase-3 activity in live tumor-bearing animals dynamically over time, our results support the concept that activation of AKT contributes to cisplatin resistance and likely results from prior exposure to the agent.

Activation of AKT is regulated by various factors, including insulin and the DNA damage response. Several reports have thus far demonstrated that AKT's complete activation depends on its phosphorylation at Ser473 and Thr308. Interestingly, Thr308 is phosphorylated by 3-phosphoinositide-dependent kinase 1 (PDK1) (33) whereas Ser473 is likely regulated by mammalian target of rapamycin complex 2 (mTORC2) (34), DNA-PK (35) and ATM (36). Here we present data indicating that cisplatin alone or in combination with perifosine induced similar DNA damage, yet single agent treatment with cisplatin induced AKT activation and resistance to apoptosis. These findings suggest that AKT activation by cisplatin may be mediated by the DNA damage response. Supporting these findings are the results of a recent study, which demonstrated DNA-PK dependent regulation of AKT phosphorylation upon cisplatin treatment (12). However, since ATM is also activated following DNA double strand breaks and has been implicated in radiation-induced AKT activation (24), the possibility remains that ATM may also play a role in regulating AKT phosphorylation which should be the subject of further investigations.

The PI3K/AKT pathway plays an important role in the cell survival pathway. The enhanced effect which we observed following cisplatin and perifosine treatments suggests that cisplatin activates the PI3K/AKT pathway thereby preventing apoptosis. Simultaneous inhibition of AKT activity by perifosine treatment can overcome this effect resulting in apoptosis. In fact, previous studies have shown that AKT through the modulation of p53 activity as well as activation of various apoptotic factors can lead to resistance to apoptosis (37–39).

Genetically engineered OEA mouse models closely recapitulate the human disease, thereby providing an excellent opportunity to study this subtype of ovarian cancer and optimize therapeutic paradigms for future clinical investigation (13). We have recently shown that the OEAs arising in our model system are inhibited by the mTOR inhibitor rapamycin, two mechanistically distinct AKT inhibitors (perifosine and API-2), as well as cisplatin plus paclitaxel (13), but combinations of conventional with targeted therapies have not been evaluated in our model system until now. Though we have not yet tested effects of cisplatin and perifosine in GEM models of serous carcinoma, we note that a substantial fraction of high grade serous carcinomas also have activated PI3K/AKT signaling, often on the basis of amplification *PIK3CA, AKT1*, or *AKT2*(5). Hence our finding that cisplatin plus perifosine is more effective than either agent alone, may apply to other ovarian cancer subtypes besides the subset of endometrioid carcinomas with activated PI3K/AKT signaling. We also note that other chemotherapeutic agents used to treat ovarian cancers, including paclitaxel, have also been shown to activate PI3K/AKT signaling (40). In addition, inhibition of PI3K has been shown to increase efficacy of paclitaxel in ovarian cancer model systems (41). Even more recently, perifosine plus docetaxel were used to treat patients with platinum and taxane resistant or refractory ovarian carcinomas in a Phase I clinical trial (42). Interestingly, all four (of 21) patients who achieved partial remission or stable disease had either endometrioid or clear cell carcinomas, and two had mutations predicted to activate PI3K/AKT signaling. Clearly, more work is required to determine whether activation of AKT by cisplatin or paclitaxel is a drug-specific or more general effect, and to define the tumor subsets most likely to respond to therapeutic regimens including PI3K/AKT pathway inhibitors.

Monitoring tumor progression and molecular events in intra-abdominal tumors usually involves sacrificing large number of animals for traditional biochemical assays. In order to enable the detection of molecular events within tumors longitudinally, we utilized our previously developed bioluminescence reporters along with anatomical- and DW-MR imaging. The use of the bioluminescence reporters provided for the ability to quantify the extent of apoptosis and AKT activation over time. We demonstrated *in vivo* that repeated

cycles of cisplatin treatment resulted in AKT activation, thus revealing molecular mechanisms that contribute to the development of cisplatin resistance. The combination of cisplatin and perifosine was able to inhibit AKT activity and overcome resistance to cisplatin through apoptotic induction and therefore may present a more effective therapeutic paradigm for the treatment of ovarian patients.

Although bioluminescence imaging represents a vital tool for imaging molecular events in animal models, it has its limitations in the clinical settings. In order to develop an imaging biomarker that can be clinically translated for use with ovarian cancer patients, we evaluated the application of DW-MRI as a surrogate for detection of treatment associated loss of tumor cellularity. DW-MRI has shown promise as a surrogate biomarker of therapeutic response with correlations to survival outcomes in cancer patients (27, 43, 44). In our study, DW-MRI revealed that both high doses of cisplatin and in combination with perifosine, significant loss of tumor cellularity occurs in contrast to treatment using perifosine alone which was found to have a minimal effect on reducing tumor cell density.

In summary, animal models with defined mutations in key signaling pathways are powerful tools to provide a better understanding of therapeutic efficacy of single agents and to explore the efficacy of combination therapeutic strategies. Molecular imaging technologies such as bioluminescence imaging of mouse models as well as MRI in pre-clinical and clinical studies not only provide an accurate and non-invasive measure of tumor burden and efficacy, but can also enable validation of drug target interactions and acquired drug resistance. Results described here provide an impetus for initiation of clinical studies with integrated DW-MRI biomarker readouts to evaluate pharmacological inhibition of the PI3K/AKT survival signaling pathway when combined with cisplatin to prevent the development of therapeutic resistance and thus significantly impact overall survival in women with OEA.

Acknowledgments

This work was supported by grants from the Department of Defense Ovarian Cancer Research Program (W81XWH-08-1-0453), the National Cancer Institute (P50-CA093990) and the National Institutes of Health (RO1CA094172). We acknowledge the late Maggie Van Keuren for preparation of the transgenic mice and the Transgenic Animal Model Core of the University of Michigan's Biomedical Research Core Facilities. Core support was provided by the University of Michigan Cancer Center, NIH grant number P30-CA046592. We acknowledge the members of the CMI for technical suggestions and critical reading of the manuscript.

References

1. Siegel R, Naishadham D, Jemal A. Cancer Statistics, 2012. Ca-a Cancer Journal for Clinicians. 2012; 62(1):10–29. [PubMed: 22237781]
2. Jemal A, Siegel R, Xu J, Ward E. Cancer statistics, 2010. CA Cancer J Clin. 2010; 60(5):277–300. [PubMed: 20610543]
3. Seidman JD, Horkayne-Szakaly I, Haiba M, Boice CR, Kurman RJ, Ronnett BM. The histologic type and stage distribution of ovarian carcinomas of surface epithelial origin. International Journal of Gynecological Pathology. 2004; 23(1):41–44. [PubMed: 14668549]
4. Rosen DG, Yang G, Liu G, Mercado-Uribe I, Chang B, Xiao XS, et al. Ovarian cancer: pathology, biology, and disease models. Front Biosci. 2009; 14:2089–102. [PubMed: 19273186]
5. Integrated genomic analyses of ovarian carcinoma. Nature. 2011; 474(7353):609–15. [PubMed: 21720365]
6. Wu R, Hendrix-Lucas N, Kuick R, Zhai Y, Schwartz DR, Akyol A, et al. Mouse model of human ovarian endometrioid adenocarcinoma based on somatic defects in the Wnt/beta-catenin and PI3K/Pten signaling pathways. Cancer Cell. 2007; 11(4):321–33. [PubMed: 17418409]
7. Bast RC Jr, Hennessy B, Mills GB. The biology of ovarian cancer: new opportunities for translation. Nat RevCancer. 2009; 9(6):415–28.

8. Kelland L. The resurgence of platinum-based cancer chemotherapy. Nature Reviews Cancer. 2007; 7(8):573–584.
9. Agarwal R, Kaye SB. Ovarian cancer: strategies for overcoming resistance to chemotherapy. Nat RevCancer. 2003; 3(7):502–16.
10. Siddik ZH. Cisplatin: mode of cytotoxic action and molecular basis of resistance. Oncogene. 2003; 22(47):7265–79. [PubMed: 14576837]
11. Cheng JQ, Lindsley CW, Cheng GZ, Yang H, Nicosia SV. The Akt/PKB pathway: molecular target for cancer drug discovery. Oncogene. 2005; 24(50):7482–7492. [PubMed: 16288295]
12. Stronach EA, Chen M, Maginn EN, Agarwal R, Mills GB, Wasan H, et al. DNA-PK mediates AKT activation and apoptosis inhibition in clinically acquired platinum resistance. Neoplasia. 2011; 13(11):1069–80. [PubMed: 22131882]
13. Wu R, Hu TC, Rehemtulla A, Fearon ER, Cho KR. Preclinical testing of PI3K/AKT/mTOR signaling inhibitors in a mouse model of ovarian endometrioid adenocarcinoma. Clin Cancer Res. 2011; 17(23):7359–72. [PubMed: 21903772]
14. Gross S, Piwnica-Worms D. Molecular imaging strategies for drug discovery and development. Current Opinion in Chemical Biology. 2006; 10(4):334–342. [PubMed: 16822702]
15. Galban CJ, Galban S, Van Dort ME, Luker GD, Bhojani MS, Rehemtulla A, et al. Applications of molecular imaging. Prog Mol Biol Transl Sci. 2010; 95:237–98. [PubMed: 21075334]
16. Zhang L, Lee KC, Bhojani MS, Khan AP, Shilman A, Holland EC, et al. Molecular imaging of Akt kinase activity. Nat Med. 2007; 13(9):1114–9. [PubMed: 17694068]
17. Coppola JM, Ross BD, Rehemtulla A. Noninvasive imaging of apoptosis and its application in cancer therapeutics. Clin Cancer Res. 2008; 14(8):2492–501. [PubMed: 18413842]
18. Suzuki A, Yamaguchi MT, Ohteki T, Sasaki T, Kaisho T, Kimura Y, et al. T cell-specific loss of Pten leads to defects in central and peripheral tolerance. Immunity. 2001; 14(5):523–34. [PubMed: 11371355]
19. Shibata H, Toyama K, Shioya H, Ito M, Hirota M, Hasegawa S, et al. Rapid colorectal adenoma formation initiated by conditional targeting of theApc gene. Science. 1997; 278(5335):120–3. [PubMed: 9311916]
20. Anton M, Graham FL. Site-specific recombination mediated by an adenovirus vector expressing the Cre recombinase protein: a molecular switch for control of gene expression. J Virol. 1995; 69(8):4600–6. [PubMed: 7609024]
21. Dinulescu DM, Ince TA, Quade BJ, Shafer SA, Crowley D, Jacks T. Role of K-ras and Pten in the development of mouse models of endometriosis and endometrioid ovarian cancer. Nat Med. 2005; 11(1):63–70. [PubMed: 15619626]
22. Flesken-Nikitin A, Choi KC, Eng JP, Shmidt EN, Nikitin AY. Induction of carcinogenesis by concurrent inactivation of p53 and Rb1 in the mouse ovarian surface epithelium. Cancer Res. 2003; 63(13):3459–63. [PubMed: 12839925]
23. Kondapaka SB, Singh SS, Dasmahapatra GP, Sausville EA, Roy KK. Perifosine, a novel alkylphospholipid, inhibits protein kinase B activation. Molecular Cancer Therapeutics. 2003; 2(11):1093–1103. [PubMed: 14617782]
24. Bozulic L, Surucu B, Hynx D, Hemmings BA. PKB alpha/Akt1 acts downstream of DNA-PK in the DNA double-strand break response and promotes survival. Molecular Cell. 2008; 30(2):203–213. [PubMed: 18439899]
25. Frese KK, Tuveson DA. Maximizing mouse cancer models. Nat Rev Cancer. 2007; 7(9):645–58. [PubMed: 17687385]
26. Becher OJ, Holland EC. Genetically engineered models have advantages over xenografts for preclinical studies. Cancer Res. 2006; 66(7):3355–8. discussion 3358–9. [PubMed: 16585152]
27. Hamstra DA, Rehemtulla A, Ross BD. Diffusion magnetic resonance imaging: a biomarker for treatment response in oncology. J Clin Oncol. 2007; 25(26):4104–9. [PubMed: 17827460]
28. Galban S, Lemasson B, Williams TM, Li F, Heist KA, Johnson TD, et al. DW-MRI as a biomarker to compare therapeutic outcomes in radiotherapy regimens incorporating temozolomide or gemcitabine in glioblastoma. PLoS One. 2012; 7(4):e35857. [PubMed: 22536446]
29. Galluzzi L, Senovilla L, Vitale I, Michels J, Martins I, Kepp O, et al. Molecular mechanisms of cisplatin resistance. Oncogene. 2012; 31(15):1869–1883. [PubMed: 21892204]

30. Stommel JM, Kimmelman AC, Ying H, Nabioullin R, Ponugoti AH, Wiedemeyer R, et al. Coactivation of receptor tyrosine kinases affects the response of tumor cells to targeted therapies. Science. 2007; 318(5848):287–90. [PubMed: 17872411]

31. Sancho-Martinez SM, Piedrafita FJ, Cannata-Andia JB, Lopez-Novoa JM, Lopez-Hernandez FJ. Necrotic concentrations of cisplatin activate the apoptotic machinery but inhibit effector caspases and interfere with the execution of apoptosis. Toxicol Sci. 2011; 122(1):73–85. [PubMed: 21527773]

32. Yip HT, Chopra R, Chakrabarti R, Veena MS, Ramamurthy B, Srivatsan ES, et al. Cisplatin-induced growth arrest of head and neck cancer cells correlates with increased expression of p16 and p53. Arch Otolaryngol Head Neck Surg. 2006; 132(3):317–26. [PubMed: 16549753]

33. Alessi DR, James SR, Downes CP, Holmes AB, Gaffney PR, Reese CB, et al. Characterization of a 3-phosphoinositide-dependent protein kinase which phosphorylates and activates protein kinase Balpha. Curr Biol. 1997; 7(4):261–9. [PubMed: 9094314]

34. Sarbassov DD, Guertin DA, Ali SM, Sabatini DM. Phosphorylation and regulation of Akt/PKB by the rictor-mTOR complex. Science. 2005; 307(5712):1098–101. [PubMed: 15718470]

35. Feng J, Park J, Cron P, Hess D, Hemmings BA. Identification of a PKB/Akt hydrophobic motif Ser-473 kinase as DNA-dependent protein kinase. J Biol Chem. 2004; 279(39):41189–96. [PubMed: 15262962]

36. Viniegra JG, Martinez N, Modirassari P, Losa JH, Cobo CP, Lobo V, et al. Full activation of PKB/Akt in response to insulin or ionizing radiationis mediated through ATM. Journal of Biological Chemistry. 2005; 280(6):4029–4036. [PubMed: 15546863]

37. Abedini MR, Muller EJ, Bergeron R, Gray DA, Tsang BK. Akt promotes chemoresistance in human ovarian cancer cells by modulating cisplatin-induced, p53-dependent ubiquitination of FLICE-like inhibitory protein. Oncogene. 2010; 29(1):11–25. [PubMed: 19802016]

38. Yang X, Fraser M, Moll UM, Basak A, Tsang BK. Akt-mediated cisplatin resistance in ovarian cancer: modulation of p53 action on caspase-dependent mitochondrial death pathway. Cancer Res. 2006; 66(6):3126–36. [PubMed: 16540663]

39. Fraser M, Leung BM, Yan XJ, Dan HC, Cheng JQ, Tsang BK. p53 is a determinant of X-linked inhibitor of apoptosis protein/Akt-mediated chemoresistance in human ovarian cancer cells. Cancer Research. 2003; 63(21):7081–7088. [PubMed: 14612499]

40. Le XF, Hittelman WN, Liu JX, McWatters A, Li C, Mills GB, et al. Paclitaxel induces inactivation of p70 S6 kinase and phosphorylation of Thr(421) and Ser(424) via multiple signaling pathways in mitosis. Oncogene. 2003; 22(4):484–497. [PubMed: 12555062]

41. Hu LM, Hofmann J, Lu YL, Mills GB, Jaffe RB. Inhibition of phosphatidylinositol 3′-kinase increases efficacy of paclitaxel in in vitro and in vivo ovarian cancer models. Cancer Research. 2002; 62(4):1087–1092. [PubMed: 11861387]

42. Fu SQ, Hennessy BT, Ng CS, Ju ZL, Coombes KR, Wolf JK, et al. Perifosine plus docetaxel in patients with platinum and taxane resistant or refractory high-grade epithelial ovarian cancer. Gynecologic Oncology. 2012; 126(1):47–53. [PubMed: 22487539]

43. Chenevert TL, Stegman LD, Taylor JMG, Robertson PL, Greenberg HS, Rehemtulla A, et al. Diffusion magnetic resonance imaging: an early surrogate marker of therapeutic efficacy in brain tumors. Journal of the National Cancer Institute. 2000; 92(24):2029–2036. [PubMed: 11121466]

44. Sala E, Kataoka MY, Priest AN, Gill AB, McLean MA, Joubert I, et al. Advanced Ovarian Cancer: Multiparametric MR Imaging Demonstrates Response- and Metastasis-specific Effects. Radiology. 2012; 263(1):149–159. [PubMed: 22332064]

Statement of Translational Relevance

Because many patients with ovarian cancer ultimately relapse after treatment, understanding the mechanisms by which tumor cells acquire resistance to chemotherapy is critically important and should aid in the development of novel and more effective treatment paradigms. In the present study, we used molecular imaging and a genetically engineered mouse ovarian cancer model to demonstrate that prolonged administration of cisplatin results in activation of the PI3K/AKT cell survival signaling cascade which, in turn, contributes to the therapeutic resistance of tumors. The efficacy of cisplatin was enhanced when combined with an inhibitor of the PI3K/AKT signaling pathway, compared to either agent alone. These results provide a compelling case for including PI3K/AKT signaling pathway inhibitors with cisplatin for treating ovarian cancers. We also demonstrate the utility of a magnetic resonance imaging-based predictive biomarker (ADC) to guide clinical translation.

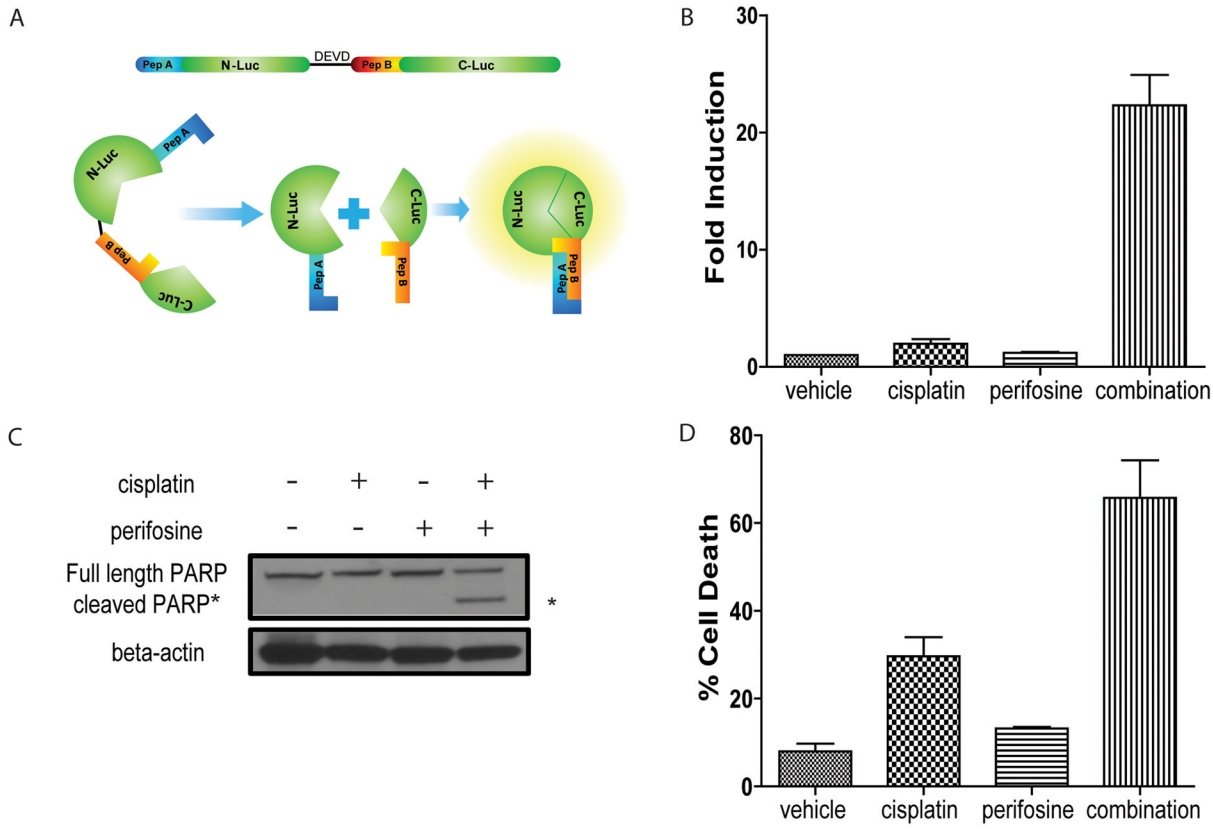

Figure 1. Perifosine sensitizes ovarian tumor cells to cisplatin-induced apoptosis

(A) Schematic of bioluminescent apoptosis reporter molecule. Wildtype luciferase was separated into two peptides, N-terminal luciferase (N-luc) and C-terminal luciferase (C-luc). The two termini were separated by a linker region and the DEVD sequence, a recognition- and cleavage site of activated caspase-3. Two strong interacting peptides, namely peptide A and peptide B were fused to N-luc and C-luc, respectively. Upon cleavage at DEVD, peptide A and peptide B overcome the hindrance created by the linker region and reconstitute wildtype luciferase activity by bringing N-luc and C-luc in proximity. **(B)** Bioluminescence assay in W25-Apop cells post 20 hours treatment with PBS, cisplatin [20 μM], perifosine [30 μM] or both of perifosine and cisplatin. Fold induction of bioluminescence signals in each group was calculated at indicated time points by normalizing bioluminescence signals to the values of vehicle group. Three independent experiments were performed and data ± SEM is depicted. **(C)** Representative western blot for PARP in W25-Apop cells treated by cisplatin and/or perifosine for 20 hours. Cleaved PARP (89 kDa) was only observed in cells treated with combination of cisplatin and perifosine. **(D)** Percent cell death was assessed by PI exclusion assay of W25-Apop cells treated for 48 hours with PBS, cisplatin [20 μM], perifosine [30 μM] or both (perifosine and cisplatin). Data was obtained from three independent experiments and represent mean ± SEM.

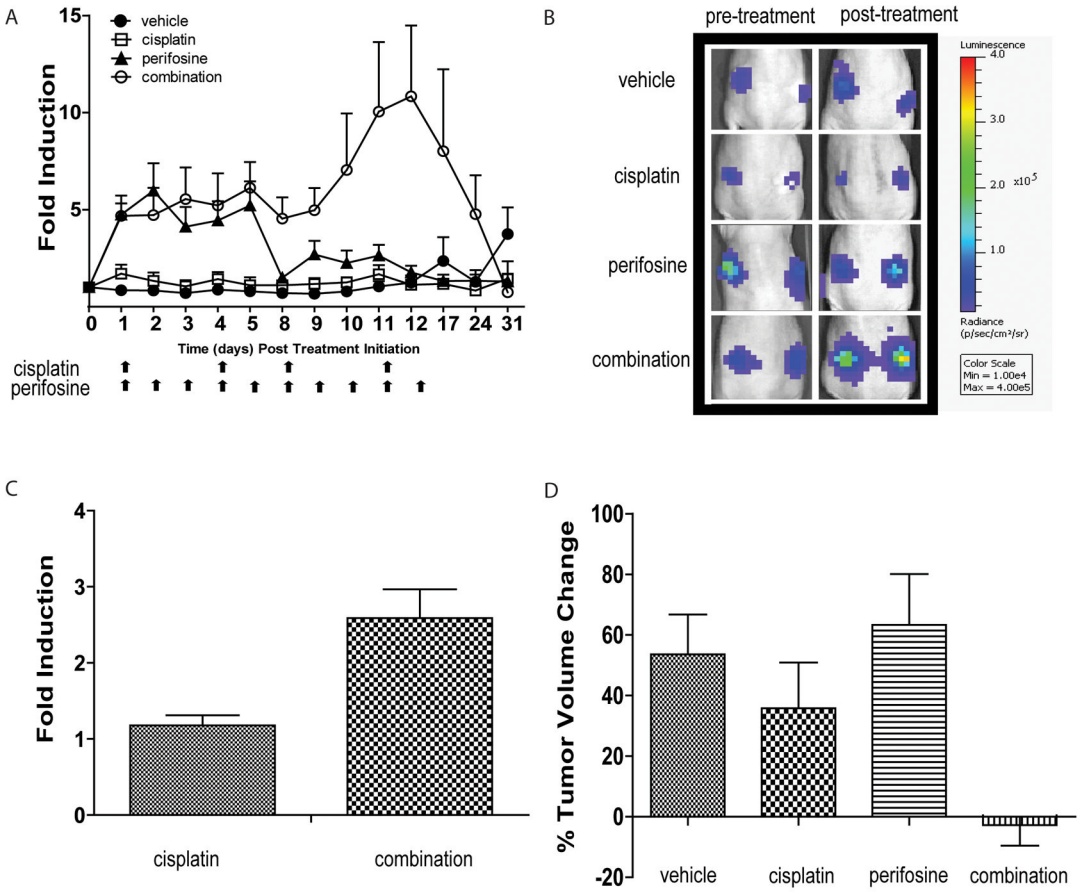

Figure 2. Induction of apoptosis in tumor allograft by combination treatment

(A) Bioluminescence imaging of W25-Apop allografts. When tumors reached ≥ 200 mm^3, animals were randomized into four treatment groups: vehicle, perifosine (10 mg/kg 5 times a week), cisplatin (5 mg/kg 2 times a week) and combination group which were treated with 5 mg/kg cisplatin 2 times a week and 10 mg/kg perifosine 5 times a week. Arrows indicate days of treatment for cisplatin and perifosine. Bioluminescence signals were normalized to tumor volumes and pre-treatment values at each time point. Mean fold induction is plotted ± SEM. **(B)** Representative BLI images pre- and post-treatment of each treatment group are shown. **(C)** Bioluminescence imaging of W25-Apop allografts at lower cisplatin doses (2.5mg/kg) at one time point (6 hours post treatment). Bioluminescence signals were normalized to pre-treatment values at each time point. Mean fold induction is plotted ± SEM. **(D)** Percent change of tumor volumes two weeks post treatment initiation. Tumor volumes were measured by caliper pre- and post-treatment. Data represent mean ± SEM.

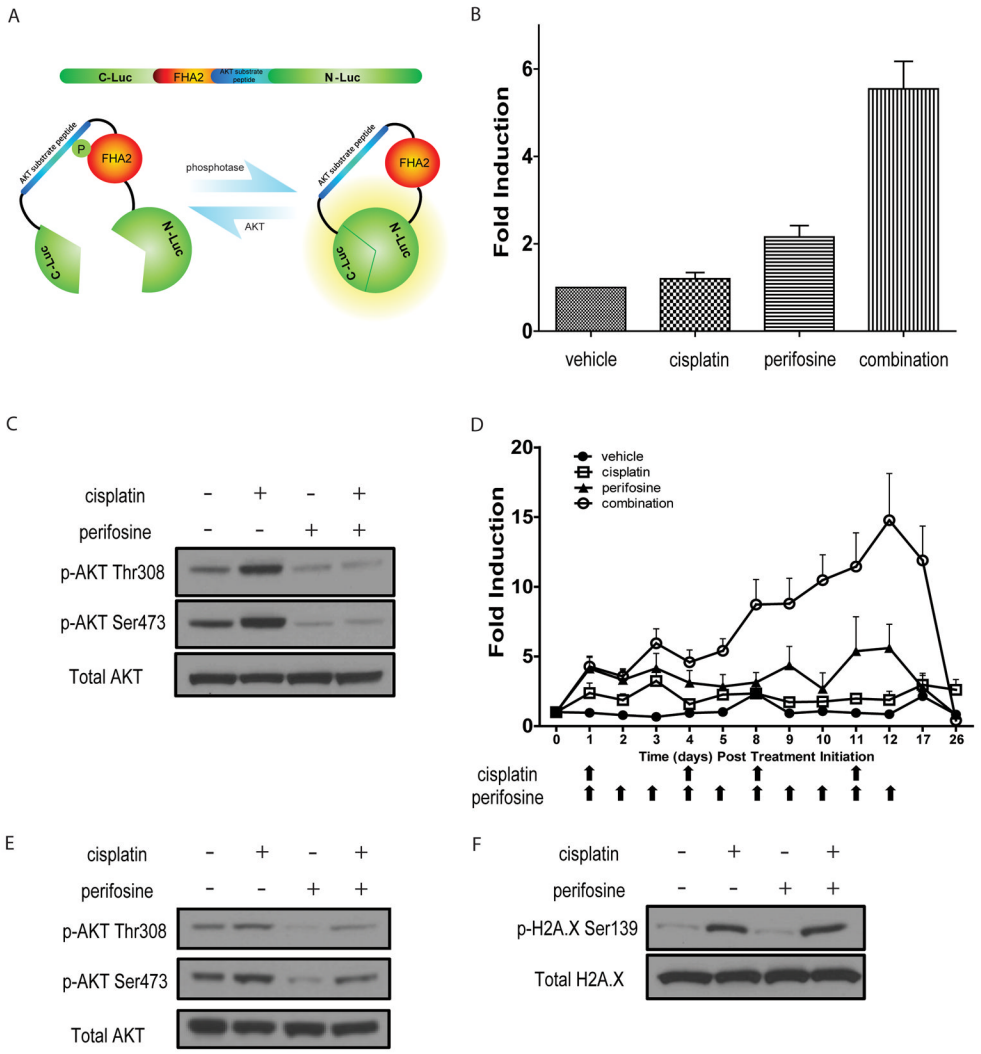

Figure 3. Increase in AKT reporter activity upon combinatorial treatment

(A) Schematic of Bioluminescence AKT Reporter (BAR). **(B)** Bioluminescence assay in W25-BAR cells post 20 hours treatment with vehicle, cisplatin [40 μM], perifosine [30 μM] or both of perifosine and cisplatin. Fold induction of bioluminescence signals in each group was calculated at indicated time points by normalizing bioluminescence signals to the values of vehicle group. Three independent experiments were performed and mean ± SEM is depicted. **(C)** Representative western blot of W25 cell lysates from vehicle-, cisplatin [40μM]-, perifosine [30μM]- or both treated cells. Antibodies against pAKT Ser473, pAKT Thr308 and total AKT were used. **(D)** Bioluminescence imaging of W25-BAR reporter allografts. When tumors reached ≥ 200 mm^3, animals were randomized into four treatment groups: vehicle, perifosine (10 mg/kg 5 times a week), cisplatin (2.5 mg/kg 2 times a week) and combination group which are treated with 2.5 mg/kg cisplatin 2 times a week and 10 mg/kg perifosine 5 times a week. Arrows indicate days of treatment for cisplatin and perifosine. Bioluminescence signals were normalized to tumor volumes and pre-treatment values at indicated time points. Mean fold induction is plotted ± SEM. **(E)** Representative images of western blot analysis of tumor tissue derived from OEA transgenic at one week post cisplatin treatment. Antibodies against pAKT Ser473, pAKT Thr308 and total AKT were used. **(F)** Representative images of western blot analysis from W25 cells treated with

vehicle, cisplatin [40 μM], perifosine [30 μM] or both. pH2A.X Ser139 and total H2A.X were detected by specific antibodies.

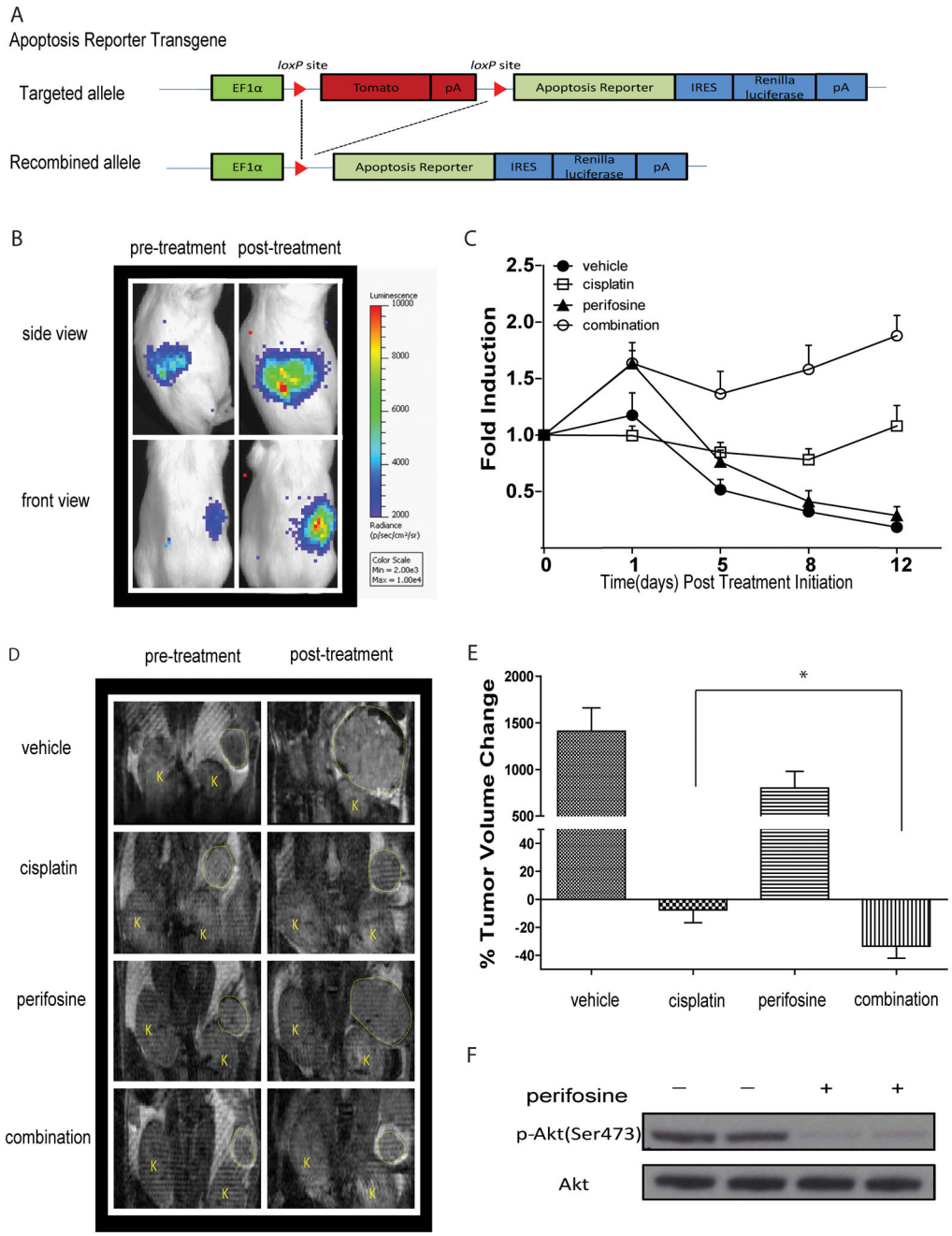

Figure 4. Generation of new reporter OEA model identifies AKT as molecular target for therapy

(A) Schematic of the bioluminescence apoptosis reporter transgene. EF-1 alpha drives expression of floxed fluorescence protein tdTomato, which is removed upon tissue specific Cre recombination. Conditional Cre recombination leads to transcription of the bioluminescent apoptosis reporter and IRES dependent renilla luciferase expression. **(B)** Representative bioluminescence images from *Apc*$^{-/-}$, *Pten* $^{-/-}$, *Apopreporter*$^{+}$ animals before treatment and one day after treatment. Bioluminescence signal is detected in the right but not left ovaries of animals. **(C)** When tumor size reached ≥ 50 mm^3 animals were randomized into four treatment groups and BL- and MR- imaging was performed before treatment and on day1, day 5, day 8 and day 12 post treatment initiation. Fold induction was

calculated by normalizing bioluminescence signals to tumor volumes acquired by MRI and pre-treatment values at each time point. Data represents mean ± SEM. **(D)** Representative MR images of animals in each group pre- and two weeks post treatment. **(E)** Percent change in tumor volume as measured by MR imaging. Data represents mean ± SEM. Statistical significance was assessed at a $p<0.05$ (*) using an unpaired Student's t-test. **(F)** Representative images of western blotting analysis for total AKT and pAKT (Ser473) 3 hours post treatment with perifosine of tumors obtained from *Apc*$^{-/-}$, *Pten* $^{-/-}$, *Apopreporter*$^{+}$ animals.

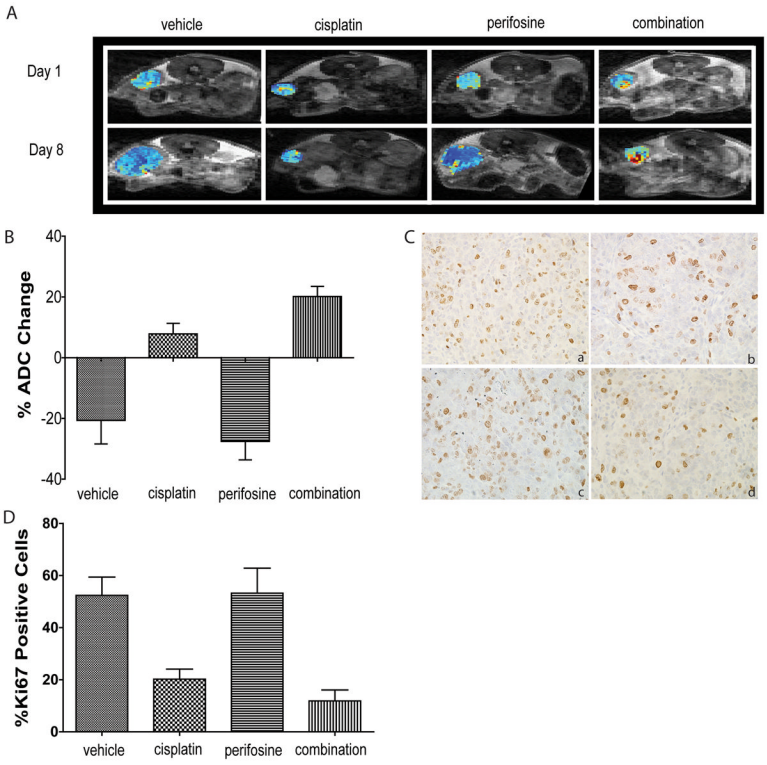

Figure 5. Diffusion MR imaging indicates cell death upon combinatorial treatment

(A) Representative ADC maps of tumor bearing *Apc*$^{-/-}$, *Pten* $^{-/-}$, *Apopreporter*$^{+}$ animals treated with vehicle, cisplatin, perifosine or combined treatment before treatment and one week after treatment. **(B)** Percent change of ADC values and statistical analysis of each treatment group after one week of treatment. Mean is plotted± SEM. **(C)** Representative images of Ki67 staining of tumor tissues from each treatment group after one week of treatment: (a) vehicle, (b) cisplatin, (c) perifosine and (d) combination. **(D)** Percent change of Ki67 stained cells of each treatment group with statistical analysis. Mean is plotted ± SEM.